

Enhanced sensing of anharmonicities in a gain-based anti-PT symmetric system

Ya-Wei Zeng(曾亚伟), Tian-Le Yang(杨天乐), Qi-Yin Lin(林琪茵), and Wan-Jun Su(苏万钧)

Citation: Chin. Phys. B, 2024, 33 (**12**): 124201. DOI: 10.1088/1674-1056/ad8a4d
Journal homepage: http://cpb.iphy.ac.cn; http://iopscience.iop.org/cpb

What follows is a list of articles you may be interested in

Frequency-modulated continuous-wave multiplexed gas sensing based on optical frequency comb calibration

Linhua Jia(贾琳华), Xinghua Qu(曲兴华), and Fumin Zhang (张福民)
Chin. Phys. B, 2024, 33 (**9**): 094201. DOI: 10.1088/1674-1056/ad5980

Design of a high sensitivity and wide range angular rate sensor based on exceptional surface

Xinsheng Ding(丁鑫圣), Wenyao Liu(刘文耀), Shixian Wang(王师贤), Yu Tao(陶煜), Yanru Zhou(周彦汝), Yu Bai(白禹), Lai Liu(刘来), Enbo Xing(邢恩博), Jun Tang(唐军), and Jun Liu(刘俊)
Chin. Phys. B, 2024, 33 (**8**): 084204. DOI: 10.1088/1674-1056/ad4324

Surface phonon resonance: A new mechanism for enhancing photonic spin Hall effect and refractive index sensor

Jie Cheng(程杰), Chenglong Wang(汪承龙), Yiming Li(李一铭), Yalin Zhang(张亚林), Shengli Liu(刘胜利), and Peng Dong(董鹏)
Chin. Phys. B, 2024, 33 (**8**): 084201. DOI: 10.1088/1674-1056/ad4a3c

Entangling two levitated charged nanospheres through Coulomb interaction

Guoyao Li(李国耀) and Zhangqi Yin(尹璋琦)
Chin. Phys. B, 2024, 33 (**7**): 074205. DOI: 10.1088/1674-1056/ad3229

Multi-functional photonic spin Hall effect sensor controlled by phase transition

Jie Cheng(程杰), Rui-Zhao Li(李瑞昭), Cheng Cheng(程骋), Ya-Lin Zhang(张亚林), Sheng-Li Liu(刘胜利), and Peng Dong(董鹏)
Chin. Phys. B, 2024, 33 (**7**): 074203. DOI: 10.1088/1674-1056/ad3b85

SPECIAL TOPIC — Quantum computing and quantum sensing

Enhanced sensing of anharmonicities in a gain-based anti-PT symmetric system

Ya-Wei Zeng(曾亚伟), Tian-Le Yang(杨天乐), Qi-Yin Lin(林琪茵), and Wan-Jun Su(苏万钧)[†]

Fujian Key Laboratory of Quantum Information and Quantum Optics and Department of Physics, Fuzhou University, Fuzhou 350116, *China*

(Received 8 September 2024; revised manuscript received 10 October 2024; accepted manuscript online 23 October 2024)

We study the enhanced sensing of weak anharmonicities in a gain-based cavity–magnon–waveguide coupled system. By dissipatively coupling the two subsystems through a mediating waveguide, the Hamiltonian of the system is tailored to be anti-parity-time symmetric. Unique to the gain condition, the eigenvalues exhibit two singularities with linewidth suppression, distinguishing them from those of gain-free systems. Under the gain condition, a counter-intuitive bistable signature emerges even at low drive powers. As the effective gain approaches a certain value, this bistability yields a significantly enhanced spin-current response of the magnon mode. Consequently, the sensitivity, quantified by an enhancement factor, is enhanced remarkably compared to the linewidth suppression scenario. Moreover, the high enhancement factor can be sustained over a broad gain-bandwidth and also stays large even when the coherent coupling becomes considerably strong. Based on the integrated cavity–magnon–waveguide systems, this scheme can be used for sensing different physical quantities related to the Kerr-type nonlinearity and has potential applications in high-precision measuring microwave-signal nonlinearities.

Keywords: sensing, nonlinearities, anti-parity-time symmetry, bistability

PACS: 42.65.Pc, 47.20.Ky, 84.40.Xb **DOI:** 10.1088/1674-1056/ad8a4d

1. Introduction

Sensing has become a prominent topic in measurements,[1] finding applications across various fields of physics, including magnetics,[2–4] optics,[5–8] electronics,[9,10] etc. In conventional Hermitian systems, sensitivity arises from the linear response manifested in resonant spectrum shifts. In recent decades, non-Hermitian dynamics[11–17] have emerged as a new approach for engineering the responses of open physical systems, with applications extending to sensing technology. Significant experimental and theoretical advancements have been achieved in exploring parity–time (PT) symmetry physics in diverse physical systems, these typically involve manipulating linear gain and loss in classical wave systems.[18–22] Concurrently, investigations into anti-parity-time (anti-PT) symmetric systems, characterized by equal effective gain or loss rates, have also progressed.[23–33] The spectral degeneracies induced by such non-Hermitian systems are known as exceptional points (EPs) where the real parts and the corresponding imaginary parts of certain eigenvalues coincide, as well as their associated eigenvectors.[34,35] Consequently, any external perturbation of system parameters across the EPs triggers phase transitions between the PT (or anti-PT) symmetric phase and broken PT (or anti-PT) symmetric phase. The sudden phase transitions have been exploited in a variety of setups and principles, such as phonon laser,[36,37] Sagnac effect,[38,39] level attraction,[40,41] and topological physics.[42–46]

It is noteworthy that sensitivity enhancement based on EPs in PT symmetric systems has been demonstrated to the perturbation ϵ, the sensitivity scaling is given by $|\partial\omega/\partial\epsilon| = |\epsilon|^{-1/2}$, where ω is the frequency splitting of the eigenmodes.[47–49] Recently, a landmark work, based on the concepts of anti-PT symmetry and the singularity named vacuum induced coherence (VIC), proposed a method for sensing Kerr nonlinearities at low drive powers.[3] The VIC singularity is characterized by the vanishing of the imaginary part of one eigenvalue, i.e., linewidth suppression. In the presence of an inherent Kerr nonlinearity in yttrium iron garnet sphere (YIGs), the nonlinear response in the vicinity of this singularity can efficiently quantify the strength of the anharmonicity, the response y behaves as $|\partial y/\partial U| = |U|^{-5/3}$, with U being the strength of nonlinearity.[3] Hence, compared to PT symmetric systems, the sensitivity of the anti-PT symmetric system to inherent nonlinearities has been greatly improved.

The VIC-based sensing scheme proposed by Nair *et al.* operates in a monostable regime under the condition that the losses of modes are confined to zero.[3] However, owing to surface roughness, impurities, and defects of the materials, the system inevitably experiences mode-dependent losses. These losses can sharply diminish the response and sensitivity to anharmonicities. Inspired by this scheme, but with a different approach, in our work effective gains are introduced to enable the system to meet the linewidth suppression condition. We concentrate on the enhanced sensitivity to Kerr nonlineari-

[†]Corresponding author. E-mail: wanjunsu@fzu.edu.cn

© 2024 Chinese Physical Society and IOP Publishing Ltd.

ties in a gain-based anti-PT symmetric system, where a cavity and a YIG sphere are coupled purely dissipatively through a mediating waveguide. With the help of gains in both modes, the system exhibits two singularities featuring linewidth suppression. Concerning stability, one of the singularities operates in the stable regime. The singularity is similar to the VIC singularity in nature, exhibiting an extraordinary sensitivity to nonlinearities.[3] Moreover, in terms of bistability, these nonlinearities can lead to bistable responses even at low drive powers under the gain condition. Taking advantage of this bistable characteristic, the sensitivity measured by an enhancement factor can be improved significantly. Furthermore, our sensing scheme demonstrates a notable robustness against fluctuations of the gain and effectively resists a relatively strong coherent coupling. Hence, this high-precision sensing might pave the way for the development of advanced sensing techniques for a wide class of systems, such as quantum dots coupled to plasmonic excitations in a nanowire,[50] quantum emitters coupled to metamaterials,[51,52] optomechanical systems,[53] hybrid magnon–photon systems,[54] and more. Additionally, the scheme has potential applications in measuring single-photon coupling strength[29] as well as microwave-signal nonlinearities.

2. Theoretical model

First, let us introduce a theoretical model of PT or anti-PT symmetric systems. The coupled system serves to realize PT and anti-PT symmetry, corresponding to two distinct interaction scenarios: coherent coupling and dissipative coupling. The behavior of such a coupled system is given by the Hamiltonian matrix

$$H = \begin{bmatrix} A+\mathrm{i}B & g-\mathrm{i}\Gamma \\ g-\mathrm{i}\Gamma & C+\mathrm{i}D \end{bmatrix}, \tag{1}$$

where A and C are the real frequencies of the respective modes, while B and D denote the effective gain or loss rates. The parameter g represents the strength of the Hermitian coherent coupling between the two modes while $\mathrm{i}\Gamma$ introduces an indirect coupling mediated by the traveling wave. Here, we employ the parity operator P and the time-reversal complex conjugate operator T. The complete condition of the PT symmetry requires specific fulfillments of parameters: $A = C$, $B = -D$, $g \neq 0$, $\Gamma = 0$, leading to the commutation relation $[PT, H] = 0$. While an anti-PT symmetric system can be realized with the following parameter configurations: $A = -C$, $B = D$, $\Gamma \neq 0$, $g = 0$, corresponding to a purely dissipatively coupled system featuring the anti-commutation relation $\{PT, H\} = 0$.

Here, as schematically shown in Fig. 1, we consider a physical model for an anharmonic two-mode system. The system comprises a YIG sphere magnon mode b of frequency ω_b and a microwave cavity photon mode a of frequency ω_a, which are coupled through a waveguide. The system can be described by the following Hamiltonian:

$$\begin{aligned} H/\hbar =\ & \omega_a a^\dagger a + \omega_b b^\dagger b + g(ab^\dagger + a^\dagger b) + U(b^{\dagger 2} b^2) \\ & + \mathrm{i}\Omega(b^\dagger \mathrm{e}^{-\mathrm{i}\omega_\mathrm{d} t} - b\,\mathrm{e}^{\mathrm{i}\omega_\mathrm{d} t}), \end{aligned} \tag{2}$$

where g is the coherent coupling strength. In our scheme, g is dropped due to the nonexistent spatial overlap between the cavity and magnon modes. U is the strength of Kerr nonlinearity intrinsic to the magnon mode b. The frequency of the magnonic Kittel mode $\omega_b = \gamma_\mathrm{e} B_0$ ranges from several hundreds of MHz to tens of GHz by tuning the biased magnetic field B_0. An external laser at frequency ω_d is applied to drive the magnon mode, with the Rabi frequency given by $\Omega = \frac{\gamma_\mathrm{e}}{2}\sqrt{\frac{5\mu_0 \rho_\mathrm{e} d D_\mathrm{p}}{3c}}$, where D_p is the corresponding drive power. The Fe^{3+} ion density and the diameter of the YIG are given by $\rho_\mathrm{e} = 4.22 \times 10^{27}$ m^{-3} and $d = 1$ mm, respectively. $\mu_0/2\pi = 2 \times 10^{-7}$ N/A^2 is the vacuum magnetic permeability. $\gamma_\mathrm{e}/2\pi = 28$ GHz/T denotes the gyromagnetic ratio for electron spin, and $c = 1 \times 10^8$ m/s is the speed of light.

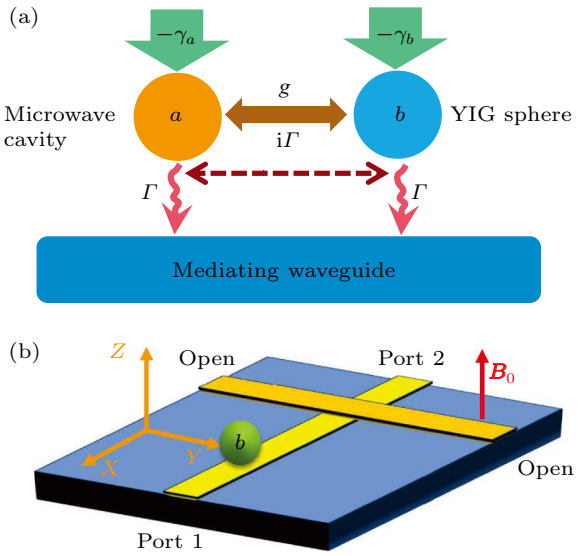


Fig. 1. (a) Schematic diagram of a general two-mode system with external gains. A microwave cavity mode a and a YIG magnon mode b are coupled to a waveguide (shared bath) with the strength Γ, and an indirect dissipative coupling $\mathrm{i}\Gamma$ is introduced between the two subsystems. g is the coherent coupling strength. $-\gamma_a$ and $-\gamma_b$ are the effective gain rates of a and b. (b) Schematic of the cavity–magnon setup. The microwave cavity, running transverse to the waveguide, interacts with the YIG via the mediating waveguide (yellow transmission line). The Kittel mode of the magnon mode is generated by a static magnetic field B_0.

The intrinsic losses of both the cavity and magnon modes will inevitably be formed, having negative effects on the realization of the linewidth suppression.[3] To address this problem, we introduce the external gains and let the gains compensate for the mode losses. Specifically, by defining the gain (damping) rates for the cavity and magnon modes as P_a (κ_a) and P_b (κ_b), respectively, the effective gain coefficients $-\gamma_a = -\kappa_a + P_a$ and $-\gamma_b = -\kappa_b + P_b$ can be obtained. Assuming the system works at zero temperature, the noise terms

average out to zero. The mean-value dynamics of the system are derived by solving the master equation in the Lindblad form, which is given by the following equation in terms of the density matrix ρ:

$$\frac{\mathrm{d}\rho}{\mathrm{d}t} = -\frac{\mathrm{i}}{\hbar}[H,\rho] + \gamma_a \mathcal{L}(a)\rho + \gamma_b \mathcal{L}(b)\rho + 2\Gamma\mathcal{L}(c)\rho, \quad (3)$$

where the second and the third terms on the right-hand side of Eq. (3) represent the effective losses or gains (determined by the sign of γ_j ($j = a,b$)) of the two modes a and b, respectively. The fourth term accounts for the cooperative interactions induced by the mediating effect of the shared reservoir. $\mathcal{L}$ is the Liouvillian operator defined by its action $\mathcal{L}(\sigma)\rho = 2\sigma\rho\sigma^\dagger - \sigma^\dagger\sigma\rho - \rho\sigma^\dagger\sigma$. The jump operator m is a linear superposition of the annihilation operators a and b, which is determined by $m = va + u\mathrm{e}^{\mathrm{i}\theta}b$, where the coefficients v and u characterize the individual couplings of the cavity and magnon modes with the traveling wave, and $\mathrm{e}^{\mathrm{i}\theta}$ describes the relative phase between the couplings. Supposing the modes interact identically with the common reservoir, $m = (a+b)/\sqrt{2}$ is valid if the phase difference of light propagation from one mode to the other is an integral multiple of 2π, thereby introducing an effective dissipative coupling $\mathrm{i}\Gamma$. In the rotating frame of ω_d, the mode detunings $\Delta_i = \omega_i - \omega_\mathrm{d}$ ($i = a,b$). The identical effective gains (or losses) $\gamma_0 = \gamma_a = \gamma_b$ and opposite detunings $\Delta_a = -\Delta_b = \Delta$ are set as preliminary conditions for achieving anti-PT symmetry. Since $\langle\dot{o}\rangle = \mathrm{Tr}(\dot{\rho}o)$ ($o = a,b$), a simplified form of the evolution is expressed as

$$\begin{pmatrix}\dot{a}\\ \dot{b}\end{pmatrix} = -\mathrm{i}\mathcal{H}\begin{pmatrix}a\\ b\end{pmatrix} - 2\mathrm{i}U\left(b^\dagger b\right)\begin{pmatrix}0&0\\0&1\end{pmatrix}\begin{pmatrix}a\\ b\end{pmatrix} + \Omega\,\mathrm{e}^{-\mathrm{i}\omega_\mathrm{d}t}\begin{pmatrix}0\\1\end{pmatrix},$$

with

$$\mathcal{H} = \begin{pmatrix}\Delta - \mathrm{i}(\gamma_0+\Gamma) & -\mathrm{i}\Gamma\\ -\mathrm{i}\Gamma & -\Delta - \mathrm{i}(\gamma_0+\Gamma)\end{pmatrix}$$

being an anti-PT symmetric matrix. Here, the mean-field approximation $\langle c_1 c_2\rangle = \langle c_1\rangle\langle c_2\rangle$ is applied for any pair of operators to handle the nonlinear term. Prior to advancing to a more generalized treatment, we initially ignore the nonlinear term U, and will incorporate it subsequently. The steady-state solutions, α and β, for the mean values of a and b, would unfold respectively as

$$\alpha = \frac{\Gamma}{\Gamma^2 - \Delta^2 - (\gamma_0+\Gamma)^2}\Omega,$$
$$\beta = \frac{-\mathrm{i}\Delta - (\gamma_0+\Gamma)}{\Gamma^2 - \Delta^2 - (\gamma_0+\Gamma)^2}\Omega. \quad (4)$$

It is evident that the linear response can diverge when the denominators of Eq. (4) approach zero (i.e., $\Gamma^2 - \Delta^2 - (\gamma_0 + \Gamma)^2 \to 0$). This intriguing characteristic suggests the system possesses an infinite sensing potential for system parameters such as Δ and γ_0.[14]

3. Linewidth suppression

As previously discussed, an anti-PT symmetric realization of modes hybridization can be precisely identified in the rotating frame if the two modes retain their loss or gain nature, fulfilling $(PT)\mathcal{H}(PT) = -\mathcal{H}$. The corresponding eigenvalues of $\mathcal{H}$ are

$$\lambda_\pm = \begin{cases} -\mathrm{i}(\gamma_0+\Gamma) \pm \mathrm{i}\sqrt{\Gamma^2 - \frac{\delta^2}{4}}, & |\frac{\delta}{2}| < \Gamma, \\ -\mathrm{i}(\gamma_0+\Gamma) \pm \sqrt{\frac{\delta^2}{4} - \Gamma^2}, & |\frac{\delta}{2}| > \Gamma, \end{cases} \quad (5)$$

where $\delta = 2\Delta$. EPs appear at $|\delta/2| = \Gamma$. The phenomenon of phase transition occurs on either side of the EPs. The region where $|\delta/2| < \Gamma$ corresponds to the anti-PT symmetric phase, in which the two eigenvalues are purely imaginary. In the anti-PT symmetry broken phase $|\delta/2| > \Gamma$, the two eigenvalues possess equal imaginary parts but different real parts.

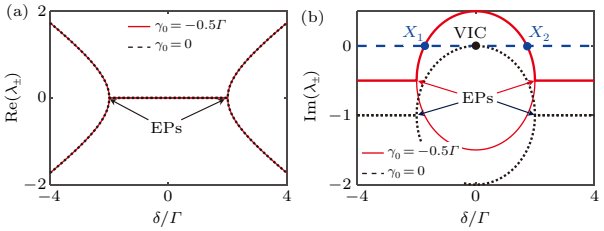


Fig. 2. (a) Real parts (eigenfrequencies) and (b) imaginary parts (linewidths) for an anti-PT symmetric system, plotted as functions of δ, with $\gamma_0 = 0$ (the black dotted line) and -0.5Γ (the red solid line). The blue dashed line highlights the points which correspond to the VIC or gain-induced linewidth suppression, with VIC point at $\delta = 0$ and X_1 at $\delta = -1.732\Gamma$ (X_2 at $\delta = 1.732\Gamma$).

In the anti-PT symmetric phase, the eigenvalues are given by $\lambda_\pm = -\mathrm{i}(\gamma_0+\Gamma) \pm \mathrm{i}\sqrt{\Gamma^2 - \frac{\delta^2}{4}}$. What interests us is the eigenvalue with a vanishing imaginary part (i.e., linewidth suppression). When $(\gamma_0+\Gamma) > \Gamma$ ($\gamma_0 > 0$, which means the inevitable intrinsic losses in gain-free systems), the precise condition for linewidth suppression cannot be met. This implies that the linewidth suppression signature would be absent in a gain-free system. However, since $\mathrm{Re}(\lambda_\pm) = 0$, in our gain-based system, where the effective gain rate is engineered from 0 to Γ for stability reasons, we find that the linewidth suppression condition is

$$\lambda_+ \to 0, \quad (6)$$

which can be transformed into a parameter-dependent form

$$\Gamma^2 - (\gamma_0+\Gamma)^2 - \frac{\delta^2}{4} \longrightarrow 0. \quad (7)$$

Surprisingly, Eq. (7) aligns with the divergent condition of the steady-state solutions in Eq. (4). To see the linewidth suppression behavior clearly, we plot the real and imaginary parts of eigenvalues Eq. (5) against the detuning in Fig. 2. For $\gamma_0 = 0$, a singularity at $\delta = 0$ emerges, corresponding to linewidth suppression induced by VIC. This feature is essential for the sensing of weak anharmonicities.[3] For our gain-based system,

choosing $\gamma_0 = -0.5\Gamma$, two singularities, labeled X_1 and X_2, are in accord with the linewidth suppression condition. Logically, these two singularities exhibit similarities to the VIC point because of their vanishing imaginary parts. Inspired by the VIC-based sensing, the singularities in our gain-based system may also hold potential for sensing nonlinear effects.

4. Bistability in gain condition

Suppose an electromagnetic field is coupled with a nonlinear resource, the stationary response of this composite system will yield nonunique stable states if the given input is beyond a threshold power.[55] To demonstrate the enhanced sensing of Kerr nonlinearities in the gain-based system, we include the nonlinearity term U as a perturbative probe and examine the classical equation of motions for the mean (steady-state) values. In what follows, we aim to derive the critical values for mode detunings and gain rates necessary for inducing bistability.

In the rotating frame, the equations describing the modified steady-state relations are given by

$$\begin{aligned} 0 &= -\left(\mathrm{i}\frac{\delta}{2}+\gamma_0+\Gamma\right)\alpha-\Gamma\beta, \\ 0 &= -\left(-\mathrm{i}\frac{\delta}{2}+\gamma_0+\Gamma\right)\beta-2\mathrm{i}U|\beta|^2\beta-\Gamma\alpha+\Omega. \end{aligned} \tag{8}$$

Eliminating α, the spin-current response $y=|\beta|^2$ is found to satisfy a cubic relation

$$4U^2y^3+\frac{2\delta BU}{(\gamma_0+\Gamma)^2+\frac{\delta^2}{4}}y^2+\frac{B^2}{(\gamma_0+\Gamma)^2+\frac{\delta^2}{4}}y=I, \tag{9}$$

where $B=\Gamma^2-(\gamma_0+\Gamma)^2-\frac{\delta^2}{4}$ and $I=\Omega^2$. The critical condition for bistability is determined by the relation $\mathrm{d}\delta/\mathrm{d}y=\mathrm{d}^2\delta/\mathrm{d}y^2=0$.[55] The solutions of $\mathrm{d}\delta/\mathrm{d}y=0$ are

$$y_\pm=\frac{-4B}{6U[4(\gamma_0+\Gamma)^2+\delta^2]}\left[\delta\pm\sqrt{\frac{\delta^2}{4}-3(\gamma_0+\Gamma)^2}\right]. \tag{10}$$

With $U>0$, equation (10) can enable a bistable response under the following conditions: $\delta^2>12(\gamma_0+\Gamma)^2$ and $B<0$, $\delta>0$ ($B>0$, $\delta<0$). The appropriate magnitude of δ pertains to the inflection point in the δ–y graph. As for the condition $\mathrm{d}^2\delta/\mathrm{d}y^2=0$, we arrive at

$$y=\frac{-4B\delta}{6U[4(\gamma_0+\Gamma)^2+\delta^2]}. \tag{11}$$

The relation $\mathrm{d}\delta/\mathrm{d}y=\mathrm{d}^2\delta/\mathrm{d}y^2=0$ means the merging of two turning points into a single point, leading to the critical condition for bistability. The resultant critical values of δ and γ_0 satisfy $\delta^2=12(\gamma_0+\Gamma)^2$, and the critical values of detunings are then given by

$$\delta_\pm^{(\mathrm{c})}=\begin{cases}\frac{3}{2}[(2IU)^{\frac{1}{3}}+\sqrt{(2IU)^{\frac{2}{3}}+\frac{4}{3}\Gamma^2}], & \delta>0,\\ \frac{3}{2}[(2IU)^{\frac{1}{3}}-\sqrt{(2IU)^{\frac{2}{3}}+\frac{4}{3}\Gamma^2}], & \delta<0.\end{cases} \tag{12}$$

Setting $\gamma=\gamma_0+\Gamma$ for convenience, the corresponding $\gamma_\pm^{(\mathrm{c})}$ are

$$\gamma_\pm^{(\mathrm{c})}=\begin{cases}\frac{\sqrt{3}}{4}[+(2IU)^{\frac{1}{3}}+\sqrt{(2IU)^{\frac{2}{3}}+\frac{4}{3}\Gamma^2}], & \delta>0,\\ \frac{\sqrt{3}}{4}[-(2IU)^{\frac{1}{3}}+\sqrt{(2IU)^{\frac{2}{3}}+\frac{4}{3}\Gamma^2}], & \delta<0.\end{cases} \tag{13}$$

Given that the product $IU\neq 0$ for a specific drive power, the first (second) equation in Eq. (13) discloses the critical value $\gamma_+^{(\mathrm{c})}>0.5\Gamma$ for $\delta>0$ ($\gamma_-^{(\mathrm{c})}<0.5\Gamma$ for $\delta<0$). When the product IU is far smaller than Γ (the system works at a very weak drive power), both critical values approach 0.5Γ. Recalling that $\gamma=\gamma_0+\Gamma$, $\gamma_{0\pm}^{(\mathrm{c})}$ asymptotically reach -0.5Γ. Hence, the bistability condition can be sustained even at extremely weak drive powers when $\gamma_0<-0.5\Gamma$ (the effective gain rate exceeds 0.5Γ). This feature distinguishes our gain-based system from the conventional gain-free system ($\gamma_0>0$) where bistability occurs only with sufficiently strong drive powers.[3]

In order to provide a comprehensive description of the system across the entire gain range, figure 3 depicts the phase diagram with a drive power of $D_\mathrm{p}=10^{-3}$ W and nonlinearity strength $U/2\pi=0.78$ nHz. The white dashed line indicates the condition $\delta^2=12\gamma^2$, and the white dotted line denotes $B=0$. For $\delta>0$ ($\delta<0$), the necessary conditions for observing bistability are $\delta>2\sqrt{3}\gamma$ and $B<0$ ($\delta<-2\sqrt{3}\gamma$ and $B>0$). When the mode detuning sweeps forward, bistability occurs in two regions (the yellow regions). The critical gain rates for observing bistability are approximately $-\gamma_{0-}^{(\mathrm{c})}\approx 0.582\Gamma$ for $\delta<0$ and $-\gamma_{0+}^{(\mathrm{c})}\approx 0.402\Gamma$ for $\delta>0$. The asymmetry of bistability in the diagram with respect to δ can be attributed to the fact that the bistability condition Eq. (10) inherently depends on the sign of the detuning.

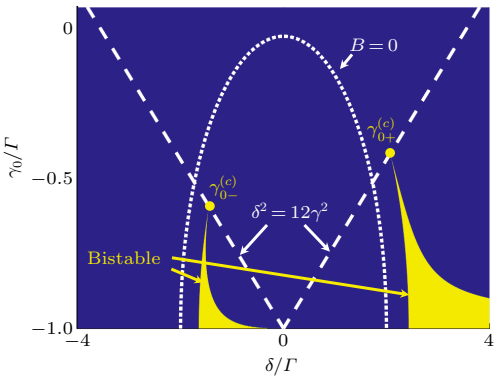


Fig. 3. The phase diagram plotted against δ and γ_0 for nonlinearity strength $U/2\pi=0.78$ nHz. Other parameters are $\Gamma/2\pi=10$ MHz and $D_\mathrm{p}=10^{-3}$ W. The white dotted line indicates the condition $\delta^2=12\gamma^2$ and the white solid line denotes $B=0$. In yellow regions, the bistability with respect to δ is asymmetric. Critical values for observing bistability are $\gamma_{0-}^{(\mathrm{c})}$ and $\gamma_{0+}^{(\mathrm{c})}$.

5. Enhanced sensing of nonlinearities

The Kerr nonlinearities can be reflected by the spin-current response of the magnon mode. When the linewidth suppression condition $B=\Gamma^2-\gamma^2-\frac{\delta^2}{4}\to 0$ is satisfied, the

second and third terms in Eq. (9) become vanishingly small, resulting in the spin-current response $y = (I/4U^2)^{1/3}$. According to this formula, the sensitivity to U is captured by the functional dependence $|\partial y/\partial U| = |U|^{-5/3}$. Therefore, a tenfold decrease in U scales up the value of y by approximately a factor of 4.64. On the other hand, for our gain-based dissipatively coupled system, examined by solving the cubic relation in Eq. (9), the spin-current response y may have one or two stable solutions within certain regions. If the second and third terms cannot be ignored, the traditional definition of the sensitivity for $\partial y/\partial U$ can no longer be given to quantify the performance of the sensing.

To provide an overview of the spin-current response encompassing both monostable and bistable regimes, figure 4(a) illustrates the rescaled response $\log_{10} y$ plotted against δ and γ_0 for the otherwise identical set of parameters as Fig. 3. An elliptic contour (depicted by the blue dotted line) is used to characterize the linewidth suppression signature. Remarkably, as the gain approaches Γ, an abnormal phenomenon of the spin-current response is noticeable, encircled by the black dashed line. The response in this region can be several orders of magnitude higher than linewidth suppression scenario. This enhancement is attributed to the enhancing effect of bistability on the spin-current response. In the following, a detailed discussion is provided to demonstrate this phenomenon and subsequently utilize this property to achieve the enhanced sensing of nonlinearities.

Before delving into the sensing of nonlinearities in the bistable regime, we first shed light on the sensitivity grounded in linewidth suppression. With a focus on the relation $|\partial y/\partial U| = |U|^{-5/3}$, figure 4(b) illustrates the relation between y and U. By inspecting the slope of the y curve, it is evident that the variation in spin-current response for a weaker nonlinearity is larger than that for a stronger nonlinearity. Essentially, it means that the spin-current response is more sensitive to a weaker nonlinearity. Thus, our scheme enables highly sensitive sensing of weak nonlinearities, which are typically elusive to conventional measurement techniques.

As the effective gain increases, the response tends to be bistable, featured by the behaviors in different gain conditions. Specifically, in Fig. 4(c), we examine the responses y against δ for different nonlinearities: $U_1/2\pi = 0.78$ nHz and $U_2/2\pi = 7.8$ nHz. When the effective gains or losses of the modes equal zero, the extreme condition $\gamma_0 = 0$ holds, giving rise to the VIC-based sensing at $\delta = 0$.[3] In this case, the response y exhibits a flat central peak near $\delta = 0$, resulting from the zero linewidth caused by vacuum induced coherence. While for $\gamma_0 = -0.5\Gamma$ in Fig. 4(d), the linewidth suppression, as characterized by the blue dotted lines, correlates with the singularities X_1 and X_2 identified in Fig. 2. As detailed above, with $\delta = 0$ serving as a reference point, the left peaks retain their monostable characteristics, while the responses on the right become bistable. Note that for both $\delta > 0$ and $\delta < 0$ regimes, denoted by the green dashed lines, the peak values of the responses exceed those at the corresponding linewidth suppression points. In this scenario, for $\delta < 0$, the response at $\delta^{(1)} = -1.465\Gamma$ attains its maximum for U_1, but fails to reach its peak for U_2, thereby yielding a more remarkable variation in y compared to the scenario of linewidth suppression. Similarly, for $\delta > 0$, the pattern persists with $\delta^{(2)} = 2.164\Gamma$. This may contribute to a more efficient sensing of nonlinearities.

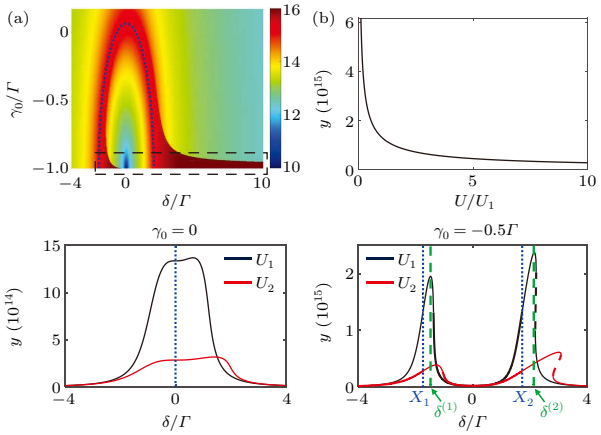


Fig. 4. The rescaled spin-current response $\log_{10} y$ plotted against δ and γ_0 for Kerr nonlinearity $U/2\pi = 0.78$ nHz. (b) The spin-current response plotted against U based on $y = (I/4U^2)^{1/3}$. (c) and (d) The spin-current responses y against δ/Γ with different γ_0. The responses in (c) are monostable, while the right peaks of the responses in (d) become bistable. The linewidth suppression is featured by the blue dotted lines. The green dashed lines mean that the spin-current response for U_1 at $\delta^{(1)} = -1.465\Gamma$ and $\delta^{(2)} = 2.164\Gamma$ reaches its peak values, and greater variations in response can be found than linewidth suppression points when a tenfold decrease in U is applied. The nonlinearity strengths are $U_1 = 2\pi \times 0.78$ nHz and $U_2 = 2\pi \times 7.8$ nHz.

Based on the fascinating feature of the spin-current response denoted in Fig. 4(a), we now proceed to investigate the distinctive features of the bistable response as effective gains approach Γ. In Fig. 5, for instance, with a gain rate 0.95Γ applied, which contrasts with the scenarios presented in Fig. 4(c) for $\gamma_0 = 0$ and Fig. 4(d) for $\gamma_0 = -0.5\Gamma$, it is demonstrated here that bistability can significantly enhance the response of y to variations in U. Furthermore, the enhancing effect becomes increasingly pronounced as the gain rate approaches Γ. For $\gamma_0 = -0.95\Gamma$, there generally exist two working regions, denoted as region I and region II, highlighted by the green region $[\delta \in (\delta_1, \delta_2) \cup (\delta_4, \delta_5)]$ and the red region $[\delta \in (\delta_2, \delta_3) \cup (\delta_5, \delta_6)]$, respectively. Here, $[\delta_1, \delta_2, \delta_3, \delta_4, \delta_5, \delta_6] = [-1.998, -1.189, -0.860, 1.998, 8.535, 72.230]\Gamma$. δ_1 and δ_4 denote the detunings associated with linewidth suppression, δ_2 (δ_5) and δ_3 (δ_6) represent the respective detunings corresponding to the turning points of the left (right) peaks for U_1 and U_2, where the upper branches terminate and the middle branches initiate. δ_2 and δ_5 are the boundaries between region I and region II. In both of these regions, bistability may be observed, thereby preventing the sensitivity from being described by a simple functional dependence $\delta y/\delta U$.

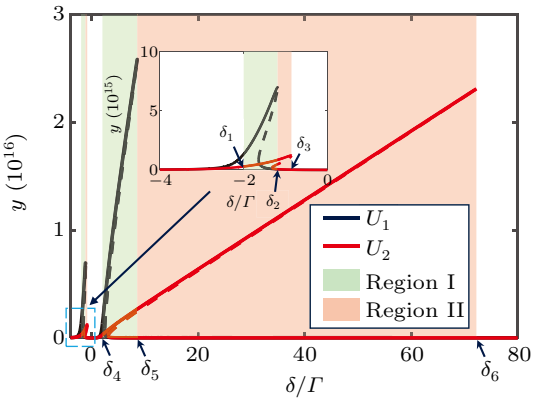


Fig. 5. The spin-current responses y plotted against δ at two different nonlinearities U_1 and U_2 for $\gamma_0 = -0.95\Gamma$. Two working regions I (denoted by the green region) and II (denoted by the red region) are given to demonstrate the different behaviors of the spin-current response. $[\delta_1, \delta_2, \delta_3, \delta_4, \delta_5, \delta_6] = [-1.998, -1.189, -0.860, 1.998, 8.535, 72.230]\Gamma$ and the other parameters are the same as those in Fig. 3.

In order to study the sensing performance in both regions, a parameter $\eta(\delta, \gamma_0)$ is introduced. This parameter, defined as the ratio of the spin-current responses $y(U_1)$ and $y(U_2)$, serves as an alternative to the conventional sensitivity measure.[29] Its concise form is

$$\eta(\delta, \gamma_0) = \frac{y(U_1)}{y(U_2)}. \tag{14}$$

The $\eta(\delta, \gamma_0)$ is called the enhancement factor. In region I, it is readily observed that $y(U_1)/y(U_2) > 1$, indicating that the factor η effectively quantifies the sensitivity. In this region, when $U_1/U_2 = 10$, $\eta(\delta, \gamma_0)$ can be significantly greater than 1. This is to be contrasted with the linewidth suppression case, where the enhancement factor is $\eta(0,0) \sim 4.64$ under an otherwise identical set of parameters. In region II, given that η is much less than 1, the inverse η^{-1} is employed as the enhancement factor instead. To generalize, we demonstrate the behavior of $\eta(\delta, \gamma_0)$ against δ and γ_0 in Fig. 6(a), where the red region signifies the increased enhancement factor η with a peak value $\eta_{\max} \sim 10$ for a tenfold decrease in U. Thus, such a factor can be regarded as an effective measure for sensing Kerr nonlinearities. Conversely, the shaded area indicates $\eta(\delta, \gamma_0) \ll 1$, which results in a large value of η^{-1}. Combined with the stability condition given analytically in Appendix A, the unstable regime is encircled by the white dashed line.

In Figs. 6(b) and 6(c), we depict the enhancement factor η and its inverse η^{-1} as functions of δ with $\gamma_0 = -0.95\Gamma$, respectively. It should be noted that the solid line indicates the enhancement factor when both responses y_1 and y_2 are stable, while the dashed line represents the enhancement factor when one or both responses are unstable. As evident in Fig. 6(b), the responses at the linewidth suppression point become unstable for $\delta > 0$, but can work in stable regime for $\delta < 0$. As revealed in Appendix A, this unusual stability behavior is determined by the modulating effect of the nonlinearity term on the mode detuning. In region I, the enhancement factor $\eta(\delta, -0.95\Gamma)$ progressively increases from δ_1 to δ_2 and from δ_4 to δ_5 for a forward sweep of the detuning. It achieves the maximum value of $\eta(\delta, -0.95\Gamma) \sim 9.67$ at $\delta = \delta_5 = 8.535\Gamma$, which is about twice as much as that observed in the case of linewidth suppression. Next, we turn to the region II, where the response y becomes monostable for $U = U_1$, while it keeps bistable for $U = U_2$, as shown in Fig. 6(c). In this region, as δ sweeps forward and across δ_2 (δ_5) for $\delta < 0$ ($\delta > 0$), the enhancement factor η approaches zero. However, its inverse (as the new enhancement factor) η^{-1} can be much larger than η. When δ is swept forward from δ_5 to δ_6, η^{-1} increases from 754 to 5.217×10^5 in an almost monotonous manner. Furthermore, figure 6(d) reveals that the high enhancement factor (the maximum η^{-1}) remains flat within a certain range of γ_0, which can be referred to as the bandwidth for measuring Kerr nonlinearities. Here, for $\delta = 8\Gamma$ (9Γ), the bandwidth is approximately 0.112Γ (0.103Γ). Benefiting from that, our gain-based coupled system can act as a highly sensitive and robust sensor.

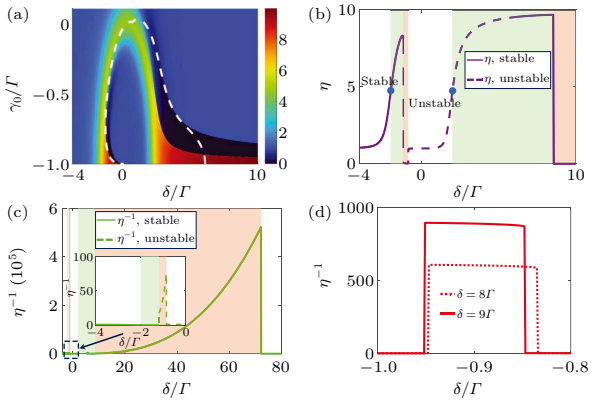


Fig. 6. (a) The enhancement factor η plotted versus the mode detuning δ and γ_0. The unstable regime is encircled by the white dashed line. (b) η plotted versus δ for the region I. (c) The enhancement factor η^{-1} plotted against δ for the region II. (d) η^{-1} plotted against γ_0 for different values of mode detuning $\delta = 8\Gamma$ and $\delta = 9\Gamma$.

The sensitivity to nonlinearities is further influenced by other parameters, such as coherent coupling and drive power. Figure 7(a) illustrates how η^{-1} varies with δ for different coherent coupling strengths $g = 0$, -0.01Γ and -0.1Γ. With a weak coherent coupling $g = -0.01\Gamma$, the peak value of the enhancement factor diminishes to 4.877×10^5 at $\delta = 70.627\Gamma$. This is owing to the fact that the coherent coupling between the two modes introduces extra linewidth, thereby leading to a reduction in the enhancement factor. Notably, for a considerably strong coherent coupling $g = -0.1\Gamma$, an effective resistance to coherent coupling can be observed because the peak of the enhancement factor can still attain a large value of 2.320×10^5 at $\delta = 55.162\Gamma$. In essence, our gain-based configuration demonstrates effective resistance against considerably strong coherent coupling. In addition, in Fig. 7(b), we plot the enhancement factors η^{-1} against δ for different drive powers $D_p = 1 \times 10^{-3}$ W and 5×10^{-4} W. Interestingly, a lower drive power yields a higher enhancement factor when

$\delta < 36.361\Gamma$ (if the system operates in stable regime), but the enhancement factor can reach a higher value for a stronger drive power within the region $\delta/\Gamma \in (36.361, 72.230)$. The introduction of gains in both modes enables us to achieve high sensitivity to Kerr nonlinearities at low drive powers and concurrently offers effective resistance against coherent coupling.

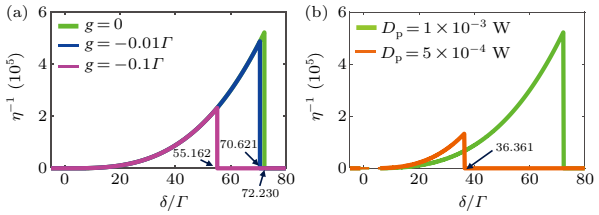


Fig. 7. (a) The enhancement factor η^{-1} plotted against δ with respect to different coherent couplings. The pink line and the blue line denote the enhancement factors for $g=-0.1\Gamma$ and $g=-0.01\Gamma$, respectively, and make a comparison with the purely dissipatively coupling case $g=0$. (b) η^{-1} plotted against the mode detuning δ for different drive powers. The green and the orange lines represent the enhancement factors at drive powers $D_p=1\times10^{-3}$ W and 5×10^{-4} W, respectively.

6. Experimental feasibility discussion

To address the experimental feasibility, we consider a magnon–cavity–waveguide hybrid system.[56–58] The Kerr nonlinearity in a YIG sphere is generated by the application of a microwave laser, which is used to drive the spatially uniform Kittel mode.[59] The Kerr nonlinearity depends on the relation $U=\mu_0 K_{an}\gamma_e^2/(M^2V_m)$, where V_m is the volume of the YIG sample, γ_e is the gyromagnetic ratio, μ_0 is the vacuum permeability, K_{an} is the first-order magnetocrystalline anisotropy constant of the YIG sphere, and M is the saturation magnetization.[58] For the YIG sphere with $R\sim1$ mm, the strength of the Kerr nonlinearity can be on the order of nanohertz.[60] The presence of these nonlinearities enables the observation of bistability.[61]

The dissipative coupling with zero coherent couplings has been engineered in previous experiments.[56] To observe bistability and implement our sensing scheme, adjusting the gain and loss rates is crucial. The physical mechanism enabling gain in a cavity has been able to be achieved by incorporating a gain element since the development of lasers.[62–64] Meanwhile, an effective gain in magnon modes can be achieved by incoherent pumping through auxiliary cavities.[65] In addition, for the YIG sphere, the damping rate is tunable by varying the position of the loop antenna which is coupled to the YIG sphere to control its damping rate on demand.[2] The natural damping of cavity mode occurs between the two open ports. By employing gain to compensate for damping, the effective gains of the modes mentioned in the main text can be realized.

7. Conclusion

In summary, it is found that, assisted by the effective gains in the microwave cavity and YIG magnon mode, the sensitivity enhancement for measuring Kerr nonlinearities can be realized in our cavity–magnon–waveguide coupled system. Engineered to be anti-PT symmetric, our gain-based system can not only exhibit strict linewidth suppression points but also show bistable behavior. Both these features positively influence the sensing scheme. Sensitivity to nonlinearities under linewidth suppression scenarios is governed by the functional dependence $|\partial y/\partial U| = |U|^{-5/3}$, distinguishing it from gain-free systems where the strict linewidth suppression condition cannot be maintained. Moreover, bistability can occur even at extremely weak drive powers in the gain condition, whereas it exists only for sufficiently strong drive powers in gain-free systems. To assess sensing performance in both monostable and bistable regimes, an enhancement factor is utilized to quantify sensitivity to nonlinearities. This factor can attain a very large value, leading to a highly sensitive sensor. Furthermore, the high enhancement factor can be sustained over a gain-bandwidth of approximately 1 MHz and remains large even when the coherent coupling strength reaches a few megahertz. Notably, a weaker drive power makes the sensor more sensitive to nonlinearities for a certain range of detuning, but a strong drive power may lead to a larger peak. Although the configuration discussed here specifically involves a YIG sphere combined with a microwave cavity, which is coupled to a transmission waveguide, the fundamental concept of our gain-assisted two-mode system is also applicable to other scenarios, including magnon–magnon coupled systems,[66,67] cavity–cavity coupled systems,[31,68] and microwave optomechanical circuits.[69]

Appendix A: Stability

A coupled dual-mode system can be dynamically unstable under a given drive power, and the dynamical instability is usually considered undesirable. To ensure the system works in the stable regime, we turn to the linearization of the dynamics equations. As given in the main text, the dynamics of the system in terms of annihilation (creation) operators can be extended as

$$\begin{aligned}
\dot{a} &= -\mathrm{i}\Delta_a a - \gamma_a a - \Gamma(a+b),\\
\dot{a^\dagger} &= \mathrm{i}\Delta_a a^\dagger - \gamma_a a^\dagger - \Gamma(a^\dagger + b^\dagger),\\
\dot{b} &= -\mathrm{i}\Delta_b b - \gamma_b b - 2\mathrm{i}Ub^\dagger bb - \Gamma(a+b) + \Omega,\\
\dot{b^\dagger} &= \mathrm{i}\Delta_b b^\dagger - \gamma_b b^\dagger + 2\mathrm{i}Ub^+b^\dagger b - \Gamma(a^+ + b^\dagger) + \Omega. \quad \text{(A1)}
\end{aligned}$$

With $\Delta=\Delta_a=-\Delta_b$, $\gamma_a=\gamma_b=\gamma_0$, and $\gamma=\gamma_0+\Gamma$; to account for quantum fluctuations, we take recourse to the linearization of the dynamics around the classical mean values of the operators, i.e., $a(t)=\alpha+\delta a(t)$ and $b(t)=\beta+\delta b(t)$. The dynamics in terms of quantum fluctuations can be further expressed as

$$\begin{aligned}
\dot{\delta a} &= (-\mathrm{i}\Delta-\gamma)\delta a - \Gamma\delta b,\\
\dot{\delta a^\dagger} &= (\mathrm{i}\Delta-\gamma)\delta a^\dagger - \Gamma\delta b^\dagger,\\
\dot{\delta b} &= (\mathrm{i}\widetilde{\Delta}-\gamma)\delta b + 2\mathrm{i}U\beta^2\delta b^\dagger - \Gamma\delta a,\\
\dot{\delta b^\dagger} &= (-\mathrm{i}\widetilde{\Delta}-\gamma)\delta b^\dagger - 2\mathrm{i}U\beta^{*2}\delta b - \Gamma\delta a^\dagger, \quad \text{(A2)}
\end{aligned}$$

where $\widetilde{\Delta} = \Delta - 4Uy$ with $y = |\beta|^2$. At a low drive power, the dynamics of the system can be considered to be characterized by a two-dimensional anti-PT symmetric matrix since the product $U|\beta|^2$ is far less than Γ. The property of the system is mostly determined by the eigenvalues of the two-dimensional matrix $\mathcal{H}$ described in the main text. This characteristic is linked to the modified spectroscopic character of the system in response to a weak probe. However, as the drive power increases, the term $U|\beta|^2$ becomes comparable to Γ and even much larger than Γ. Consequently, a more accurate description necessitates employing the higher-order matrix.

Four quadrature operators are utilized instead to describe the dynamics of the system: $\delta q_a = (\delta a + \delta a^\dagger)/\sqrt{2}$, $\delta p_a = (\delta a - \delta a^\dagger)/(\mathrm{i}\sqrt{2})$, $\delta q_b = (\delta b + \delta b^\dagger)/\sqrt{2}$, $\delta p_b = (\delta b - \delta b^\dagger)/(\mathrm{i}\sqrt{2})$. For the new basis of the quadrature operators $\delta\zeta = [\delta q_a, \delta p_a, \delta q_b, \delta p_b]^{\mathrm{T}}$, a straightforward calculation gives the following form of the dynamics:

$$\mathcal{M} = \begin{pmatrix} -\gamma & \Delta & -\Gamma & 0 \\ -\Delta & -\gamma & 0 & -\Gamma \\ -\Gamma & 0 & -\gamma - \mathrm{i}U\Lambda & -\widetilde{\Delta} - U\Xi \\ 0 & -\Gamma & \widetilde{\Delta} - U\Xi & -\gamma - \mathrm{i}U\Lambda \end{pmatrix}, \tag{A3}$$

where $\Lambda = \beta^2 - \beta^{*2}$ and $\Xi = \beta^2 + \beta^{*2}$. The eigenvalues of the matrix $\mathcal{M}$ are

$$\begin{aligned}
\lambda_1 &= -\gamma - \frac{\sqrt{[4\Gamma^2 - (\delta - 4yU)^2] - 8yU[yU + \sqrt{(\delta - 3yU)^2 - 3\Gamma^2}]}}{2}, \\
\lambda_2 &= -\gamma + \frac{\sqrt{[4\Gamma^2 - (\delta - 4yU)^2] - 8yU[yU + \sqrt{(\delta - 3yU)^2 - 3\Gamma^2}]}}{2}, \\
\lambda_3 &= -\gamma - \frac{\sqrt{[4\Gamma^2 - (\delta - 4yU)^2] - 8yU[yU - \sqrt{(\delta - 3yU)^2 - 3\Gamma^2}]}}{2}, \\
\lambda_4 &= -\gamma + \frac{\sqrt{[4\Gamma^2 - (\delta - 4yU)^2] - 8yU[yU - \sqrt{(\delta - 3yU)^2 - 3\Gamma^2}]}}{2}.
\end{aligned} \tag{A4}$$

Following consideration of the Routh–Hurwitz criterion,[70] the real parts of the eigenvalues λ_1, λ_2, λ_3, λ_4 of the matrix $\mathcal{M}$ must be strictly negative to ensure that the system is stable. Notably, λ_2 and λ_4 suggest that the system will be unstable regardless of the values of δ and γ when $\gamma < 0$ ($\gamma_0 < -\Gamma$, the effective gain is larger than Γ), as the real parts of these two eigenvalues are consistently positive.

When the product yU is far smaller than Γ, the eigenvalues of the system can be approximately simplified as $\lambda_1 = \lambda_3 = -\gamma - \sqrt{\Gamma^2 - (\delta/2)^2}$, $\lambda_2 = \lambda_4 = -\gamma + \sqrt{\Gamma^2 - (\delta/2)^2}$, which leads to the stability condition $(\delta/2)^2 + \gamma^2 - \Gamma^2 > 0$ with $\gamma > 0$. Hence, the stability can be geometrically characterized by a semi-ellipse. Inside this semi-ellipse, the system is unstable, whereas outside this semi-ellipse, the system is stable, excluding the case where $\gamma < 0$.

It is found that the semi-ellipse also agrees with the linewidth suppression condition in the main text. As the value of yU increases, the semi-ellipse distorts and appears to shift to the right along the δ axis due to the terms $\delta - 3yU$ and $\delta - 4yU$. Thus, the singularity with linewidth suppression in $\delta < 0$ can operate within a stable regime, while the singularity in $\delta > 0$ is covered by the unstable regime.

Acknowledgment

Project supported by the National Natural Science Foundation of China (Grant Nos. 11704058 and 12174058).

References

[1] Degen C L, Reinhard F and Cappellaro P 2017 *Rev. Mod. Phys.* **89** 035002
[2] Yang Y, Wang Y P, Rao J W, Gui Y S, Yao B M, Liu W and Hu C M 2020 *Phys. Rev. Lett.* **125** 147202
[3] Nair J M P, Mukhopadhyay D and Agarwal G S 2020 *Phys. Rev. Lett.* **125** 147202
[4] Schmitt S, Gefen T, Stürner F M, Unden T, Wolf G, Müller C, Scheuer J, Naydenov B, Markham M, Pezzagna S, Meijer J, Schwarz I, Plenio M , Retzker A, McGuinness L P and Jelezko F 2017 *Science* **356** 832
[5] Chen W, Kaya Özdemir Ş, Zhao G, Wiersig J and Yang L 2020 *Nature* **548** 192
[6] Hodaei H, Hassan A U, Wittek S, Garcia-Gracia H, El-Ganainy R, Christodoulides D N and Khajavikhan M 2020 *Nature* **548** 187
[7] Aspelmeyer M, Kippenberg T J and Marquardt F 2014 *Rev. Mod. Phys.* **86** 1391
[8] Ja L H, Qu X H and Zhang F M 2024 *Chin. Phys. B* **33** 094201
[9] Zhou B B, Deng W J, Wang L F, Dong L and Huang Q A 2020 *Phys. Rev. Appl.* **13** 064022
[10] Choi Y, Hahn C, Yoon J W and Song S H 2018 *Nat. Commun.* **9** 2182
[11] Xiao Z, Li H, Kottos T and Alù A 2019 *Phys. Rev. Lett.* **123** 213901
[12] Liu Z P, Zhang J, Özdemir K, Peng B, Jing H, Lü X Y, Li C W, Yang L, Nori F and Liu Y X 2016 *Phys. Rev. Lett.* **125** 147202
[13] Chen P Y and Jung J 2016 *Phys. Rev. Lett.* **117** 110802
[14] Wang J, Mukhopadhyay D and Agarwal G S 2022 *Phys. Rev. Res.* **4** 013131
[15] Wiersig J 2016 *Phys. Rev. A* **93** 033809
[16] Li Y Y, Cao Q T, Chen J H, Yu X C and Xiao Y F 2021 *Phys. Rev. Appl.* **16** 044016
[17] Li Y, Deng Z, Qin C, Wan S, Lv B, Guan C, Yang J, Zhang S and Shi J 2023 *Opt. Express* **31** 492
[18] Bender C M and Boettcher S 1998 *Phys. Rev. Lett.* **80** 5243
[19] Bender C M, Brody D C and Jones H F 2002 *Phys. Rev. Lett.* **89** 270401
[20] Bender C M, Berry M V and Mandilara A 2002 *J. Phys. A: Math. Gen.* **35** L467
[21] Xu X W, Liu Y X, Sun C P and Li Y 2015 *Phys. Rev. A* **92** 013852
[22] Lü X Y, Jing H, Ma J Y and Wu Y 2015 *Phys. Rev. Lett.* **114** 253601

[23] Yang F, Liu Y C and You L 2017 *Phys. Rev. A* **96** 053845
[24] Fang Y L, Zhao J L, Chen D X, Zhou Y H, Zhang Y and Nori F 2022 *Phys. Rev. Res.* **4** 033022
[25] Feng Z and Sun X 2022 *Phys. Rev. Lett.* **129** 273601
[26] Liu C W, Liu Y, Du L, Su W J, Wu H and Li Y 2023 *Opt. Express* **31** 9236
[27] Li Y, Peng Y G, Han L, Miri M A, Li W, Xiao M, Zhu X F, Zhao J, Alù A, Fan S and Qiu C W 2019 *Science* **364** 170
[28] Zhang H, Huang R, Zhang S D, Li Y, Qiu C W, Nori F and Jing H 2020 *Nano Lett.* **125** 147202
[29] Mukhopadhyay D, Nair J M P and Agarwal G S 2022 *Phys. Rev. B* **105** 064405
[30] Qin Y, Chen H, Luo D, Pan C, Hu H, Zhang Y and Wei D 2021 *Opt. Express* **29** 29175
[31] Luo X W, Zhang C and Du S 2022 *Phys. Rev. Lett.* **128** 173602
[32] Zhang H L, Peng M Y, Xu X W and Jing H 2022 *Chin. Phys. B* **31** 014215
[33] Geng J T, Xu S Y, Jin T, Ding S L, Yang L, Wang Y and Zhang Y G 2024 *Chin. Phys. B* **33** 014208
[34] Zhang F, Feng Y, Chen X, Ge L and Wan W 2020 *Phys. Rev. Lett.* **124** 053901
[35] Chang L, Jiang X, Hua S, Yang C, Wen J, Jiang L, Li G, Wang G and Xiao 2014 *Nat. Photon.* **8** 524
[36] Lü H, Özdemir S K, Kuang L M, Nori F and Jing H 2017 *Phys. Rev. Appl.* **8** 044020
[37] Jing H, Özdemir S K, Lü X Y, Zhang J, Yang L and Nori F 2014 *Phys. Rev. Lett.* **113** 053604
[38] Sunada S 2017 *Phys. Rev. A* **96** 033842
[39] Harder M, Yang Y, Yao B M, Yu C H, Rao J W, Gui Y S, Stamps R L and Hu C M 2018 *Phys. Rev. Lett.* **121** 137203
[40] Yang Y, Rao J W, Gui Y S, Yao B M, Lu W and Hu C M 2019 *Phys. Rev. Appl.* **11** 054023
[41] Peng Z H, Jia C X, Zhang Y Q, Yuan J B and Kuang L M 2020 *Phys. Rev. A* **102** 043527
[42] Xu H, Mason D, Jiang L and Harris J G E 2016 *Nature* **537** 80
[43] Kawabata K, Bessho T and Sato M 2019 *Phys. Rev. Lett.* **123** 066405
[44] Ergoktas M S, Soleymani S, Kakenov N, Wang K, Smith T B, Bakan G, Balci S, Principi A, Novoselov K S Ozdemir S K and Kocabas C 2022 *Science* **376** 184
[45] Cai R, Jin Y, Li Y, Rabczuk T, Pennec Y, DjafariRouhani B and Zhuang X 2022 *Phys. Rev. Appl.* **18** 014607
[46] Gu Z, Gao H, Liu T, Liang S, An S, Li Y and Zhu J 2021 *Phys. Rev. Appl.* **15** 014025
[47] Yu S, Meng Y, Tang J S, Xu X Y, Wang Y T, Yin P, Ke Z J, Liu W, Li Z P, Yang Y Z, Chen G, Han Y J, Li C F and Guo G C 2020 *Phys. Rev. Lett.* **125** 240506
[48] Sharma S, Kani A and Bhattacharya M 2022 *Phys. Rev. A* **105** 147202
[49] Özdemir Ş K, Rotter S, Nori F and Yang L 2019 *Nat. Mater.* **18** 783
[50] Wei H, Li Z P, Tian X R, Wang Z X, Cong F Z, Liu N, Zhang S P, Nordlander P, Halas N J and Xu H X 2010 *Nano Lett.* **10** 1021
[51] Lassalle E, Lalanne P, Aljunid S, Genevet P, Stout B, Durt T and Wilkowski D 2020 *Phys. Rev. A* **101** 013837
[52] Thanopulos I, Yannopapas V and Paspalakis E 2017 *Phys. Rev. B* **95** 075412
[53] Bernier A R, Tóth L D, Feofanov A K and Kippenberg T J 2018 *Phys. Rev. A* **98** 023841
[54] Harder M, Yang Y, Yao B M, Yu C H, Rao J W, Gui Y S, Stamps R L and Hu C M 2018 *Phys. Rev. Lett.* **121** 137203
[55] Nair J M P, Mukhopadhyay D and Agarwal G S 2021 *Phys. Rev. B* **103** 224401
[56] Rao J W, Wang Y P, Yang Y, Yu T, Gui Y S, Fan X L, Xue D S and Hu C M 2020 *Phys. Rev. B* **101** 064404
[57] Bhoi B, Kim B, Jang S H, Kim J, Yang J, Cho Y J and Kim S K 2019 *Phys. Rev. B* **99** 134426
[58] Wang Y P, Rao J W, Yang Y, Xu P C, Gui Y S, Yao B M, You J Q and Hu C M 2019 *Phys. Rev. Lett.* **123** 127202
[59] Wang Y P, Zhang G Q, Zhang D, Luo X Q, Xiong W, Wang S P, Li T F, Hu C M and You J Q 2016 *Phys. Rev. B* **94** 224410
[60] Xiong W, Tian M, Zhang G Q and You J Q 2022 *Phys. Rev. B* **105** 245310
[61] Shen R C, Li J, Fan Z Y, Wang Y P and You J Q 2022 *Phys. Rev. Lett.* **129** 123601
[62] Makris K G, El-Ganainy R, Christodoulides D N and Musslimani Z H 2008 *Phys. Rev. Lett.* **100** 103904
[63] Guo A, Salamo G J, Duchesne D, Morandotti R, Volatier-Ravat M, Aimez V, Siviloglou G A and Christodoulides D N 2009 *Phys. Rev. Lett.* **103** 093902
[64] Peng B, Özdemir Ş K, Lei F, Monifi F, Gianfreda M, Long G L, Fan S, Nori F, Bender C M and Yang L 2014 *Nat. Phys.* **10** 394
[65] Zhao C, Peng R, Yang Z, Chao S, Li C, Wang Z and Zhou L 2022 *Phys. Rev. A* **105** 023709
[66] Li Y, Yefremenko V G, Lisovenko M, Trevillian C, PolakovicT, Cecil T W, Barry P S, Pearson J, Divan R, Tyberkevych V, Chang C L, Welp U, Kwok W K and Novosad V 2022 *Phys. Rev. Lett.* **128** 047701
[67] Qian J, Meng C H, Rao J W, Rao Z J, An Z, Gui Y and Hu C M 2023 *Nat. Commun.* **14** 3437
[68] Cui D, Li J, Li F, Shi Z C and Yi X X 2023 *Phys. Rev. A* **107** 013709
[69] Bernier N R, Tóth L D, Feofanov A K and Kippenberg T J 2018 *Phys. Rev. A* **98** 023841
[70] DeJesus E X and Kaufman C 1987 *Phys. Rev. A* **35** 5288